The Astronomical Journal, 128:3053–3060, 2004 December

ABSOLUTE FLUX DISTRIBUTION OF THE SDSS STANDARD BD +17°4708

R. C. Bohlin and R. L. Gilliland
Space Telescope Science Institute, 3700 San Martin Drive, Baltimore, MD 21218; bohlin@stsci.edu, gillil@stsci.edu
Received 2004 June 15; accepted 2004 September 8

ABSTRACT

Secondary flux standards are established by measuring their brightness relative to primary standard stars. The *Hubble Space Telescope* (*HST*) primary standards are the three pure-hydrogen white dwarf (WD) flux standards that determine the sensitivity calibration for the Space Telescope Imaging Spectrograph. STIS observations have defined the flux of the Sloan Digital Sky Survey (SDSS) standard BD +17°4708 from 0.17 to 1.0 μm with an uncertainty of less than 0.5% relative to the *HST* primary standards, as verified by two independent sets of photometry. The two CCD cameras, HRC and WFC, in the ACS instrument package on *HST* confirm the average ratio of BD +17°4708 to the three fainter WD primary standards to better than 0.5% if a few of the ACS filter bandpasses have small wavelength shifts. With an uncertainty of less than 0.5% in the transfer of the flux calibration from the primary standards, the accuracy of the BD +17°4708 relative flux distribution is essentially the same as that of the primary WDs, that is, ~2% in the relative fluxes over the 0.17–1 μm range. Our flux distribution agrees with the SDSS fluxes to within their quoted 3% uncertainty.

Key words: stars: fundamental parameters — stars: individual (BD +17°4708) — techniques: spectroscopic

Online material: machine-readable tables

1. INTRODUCTION

The Sloan Digital Sky Survey (SDSS) is a landmark data set with several terabytes of images of the sky that are publicly available. The flux calibration of the stellar photometry derived from these SDSS images is based primarily on the flux of BD +17°4708 (Fukugita et al. 1996; Oke & Gunn 1983). To establish the relation of the Fukugita et al. flux calibration to the *Hubble Space Telescope* (*HST*) white dwarf (WD) flux scale, spectrophotometry and photometry of BD +17°4708 were obtained in 2002–2004 using the Space Telescope Imaging Spectrograph (STIS) and Advanced Camera for Surveys (ACS), respectively.

The absolute flux calibration of *HST* instrumentation is based on models of three pure-hydrogen WD stars: GD 71, GD 153, and G191-B2B (Bohlin 2000; Bohlin et al. 2001; Bohlin 2003). In particular, the non-LTE (NLTE) model fluxes produced by I. Hubeny's TLUSTY code incorporate the known physics of actual stellar atmospheres and provide the current best estimates of the shape of the flux distributions. If there are no errors in the basic physics used to determine the stellar temperatures and gravities from the Balmer line profiles or in the stellar atmosphere codes used for the models, then the uncertainty of 3000 K for the effective temperature of G191-B2B means that the relative flux should be correct to better than 2.5% from 0.13 to 1 μm and to better than 1% from 0.35 to 1 μm.

The sensitivities of the five STIS low-dispersion spectrophotometric modes have been carefully tracked since the STIS commissioning in 1997. After correcting for changing sensitivity with time (Bohlin 1999; Stys et al. 2004)[1] and for charge transfer efficiency (CTE) losses for the three STIS spectral modes on the CCD (Bohlin & Goudfrooij 2003), STIS internal repeatability is often better than 0.5% (Bohlin 2003). Thus, *HST* observations of BD +17°4708 from 1700 to 10000 Å with the three CCD modes provide absolute spectrophotometry that is preferable to ground-based flux determinations, which require corrections for atmospheric extinction that varies significantly during an observing night.

2. STIS SPECTROPHOTOMETRY

2.1. *Internal Consistency*

Observations with a resolution $R \sim 1000$ in three STIS CCD modes—from 1680 to 3060 Å (G230LB), from 2900 to 5690 Å (G430L), and from 5300 to 10200 Å (G750L)—were obtained at three epochs between 2002 September 24 and 2003 January 9 as described in Table 1. At the shortest wavelengths of G230LB, a small stray-light correction is required; namely, 0.0035 of the average signal, 0.16 e^- s^{-1}, must be subtracted from the net count rate to bring the STIS flux down to the *IUE* value of zero at 1700 Å.

Three prerequisites for establishing secondary stellar flux standards with precise absolute spectrophotometry are high-fidelity primary standards, a linear detector system, and repeatability of observations over the lifetime of the instrument. For each of the three CCD observing modes, Figure 1 shows the repeatability of the BD +17°4708 count rates after correction for all instrumental effects. This "repeatability" is the percentage "residual" in Figure 1 and is defined as $100|1 - R/\langle R\rangle|$, where R is the count rate for an individual observation and $\langle R\rangle$ is the baseline average of the three G230LB or G750L observations or the average of the six G430L observations. The total expected 1 σ uncertainty (*heavy solid lines*) combines in quadrature the counting statistics in the wavelength bins and the measured repeatability from the monitoring of AGK +81°266 since 1997. The agreement of the repeatability of the BD +17°4708 observations with the 1 σ expectations is consistent with an uncertainty of the final fluxes relative to our primary standards of less than 0.5% over most of the wavelength coverage. In the shortest-wavelength bin at 1750 Å, the flux of the F star is ~100 times fainter than the peak at 4000 Å, and two points in

[1] These and other referenced STScI internal documents can be found at one of http://www.stsci.edu/hst/acs/documents/isrs and http://www.stsci.edu/hst/stis/documents/isrs.

TABLE 1
JOURNAL OF OBSERVATIONS

Root Name	Mode	Aperture	Date	Time	Exp. Time (s)
O8H101010.....	G430L	52 × 2E1	2002 Sep 24	13:50:35	120.0
O8H101020.....	G430L	52 × 2	2002 Sep 24	13:54:45	120.0
O8H101030.....	G230LB	52 × 2	2002 Sep 24	14:03:06	971.0
O8H101040.....	G750L	52 × 2	2002 Sep 24	14:25:38	120.0
O8H102010.....	G430L	52 × 2E1	2002 Oct 24	14:42:37	120.0
O8H102020.....	G430L	52 × 2	2002 Oct 24	14:46:47	120.0
O8H102030.....	G230LB	52 × 2	2002 Oct 24	14:55:08	971.0
O8H102040.....	G750L	52 × 2	2002 Oct 24	15:17:40	120.0
O8H103010.....	G430L	52 × 2E1	2003 Jan 9	05:23:05	120.0
O8H103020.....	G430L	52 × 2	2003 Jan 9	05:27:15	120.0
O8H103030.....	G230LB	52 × 2	2003 Jan 9	05:35:36	971.0
O8H103040.....	G750L	52 × 2	2003 Jan 9	05:58:08	120.0

the 1700–1800 Å bin at 1750 Å show 3–4 times larger residuals than the expected 1 σ value shown as the heavy solid line in Figure 1. This scatter is caused by a 5% increase in the 1750 Å stellar signal between the observations on 2002 October 24 and 2003 January 9. This change in flux is less than 10^{-3} times the peak flux and is probably true stellar variability that is analogous to the solar variation in the far-UV.

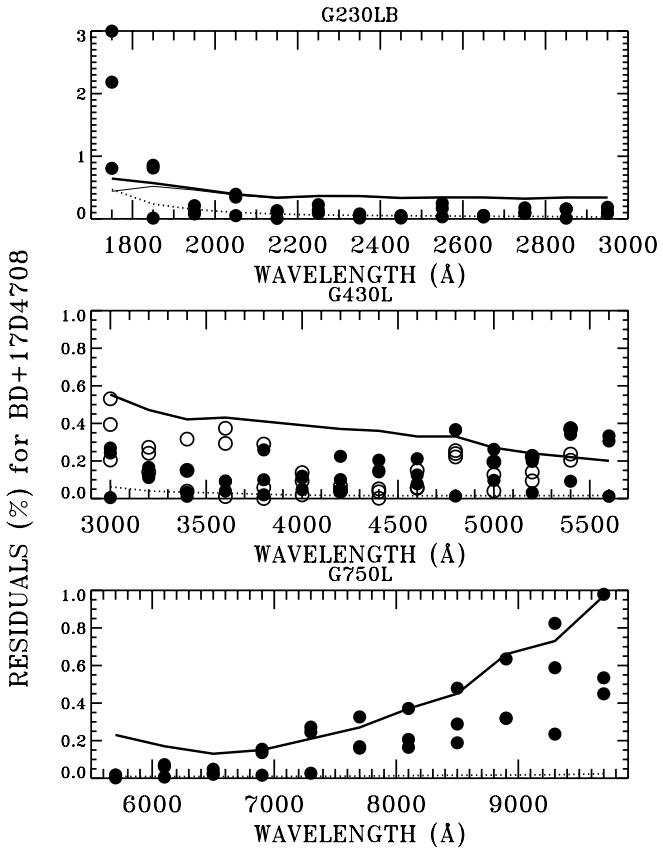

FIG. 1.—Percentage absolute values of the residuals from the comparison of the three individual observations with their average for each spectral mode at the CCD center, near row 512 (*filled circles*). For G430L, additional observations were obtained at the E1 position (*open circles*), which is only 120 pixels from the readout amplifier in order to minimize CTE losses. The bin sizes for the comparisons are 100, 200, and 400 Å for G230LB, G430L, and G750L, respectively, from top to bottom. The heavy solid lines are the total rms uncertainty from our error model. The contributions that are combined in quadrature to obtain the total uncertainty are the repeatability (*light solid line*; distinguishable from the heavy line only below 1850 Å for G230LB) and the Poisson counting statistics (*dotted line*). The light solid lines are the expected rms repeatability from a fit to the monitor observations of AGK +81°266 vs. time.

Normally, the stellar spectrum lies near the center row (512) of the CCD, but in the case of the G430L observation shown in the middle panel of Figure 1, BD +17°4708 was also observed at the position referred to as "E1," near the readout amplifier at the top of the CCD in order to minimize the CTE losses. For G230LB and G750L, uncertainty in the CTE correction does not contribute to the residuals, because all the G230LB and G750L exposures are at the same central position on the detector, have the same exposure time, and are at about the same epoch. Thus, the uncertainty in the CTE correction is relevant only for G430L. However, the high signal from the bright BD +17°4708 makes the CTE correction small; its uncertainty exceeds 0.1% only at 3000 Å, where the total signal falls below 10,000 e^-. Including the estimated uncertainty in the CTE correction of 0.5% at 3000 Å for G430L would slightly raise this one point on the solid line of Figure 1 from 0.55% to 0.7%. The trend for the E1 observations to show 0.1%–0.3% higher residuals than the centered observations at 3000–3600 Å is not significant, because the effect is only a fraction of the expected 0.5% scatter.

2.2. *Comparison with SDSS*

Fukugita et al. (1996, hereafter F96) published absolute photometry with a 20 Å bandpass for BD +17°4708, the primary SDSS standard. These fluxes are derived from the relative brightness of BD +17°4708 with respect to the primary ground-based standard, Vega. F96 analyzed previously published measures of BD +17°4708 and utilized the flux for Vega from Hayes (1985, hereafter H85). Because of the nonuniform sampling interval in this F96 flux distribution, the comparison with the STIS spectrum in narrow bands is complicated by small wavelength uncertainties and by the unknown, detailed profile of the nominal 20 Å square bandpass. However, this problematic sampling issue is unimportant for synthetic photometry in passbands that are large compared with 20 Å. Synthetic photometry is defined as the predicted count rate from the integral over the bandpass of the stellar photon flux distribution times the system-throughput quantum efficiency times the collecting area of the telescope, where the area cancels in the ratio of count rates from different flux distributions.

STIS observations of Vega (Bohlin & Gilliland 2004, hereafter BG04) and of BD +17°4708 determine their fluxes on the *HST* pure-hydrogen WD flux scale without the complications of the atmosphere and the assorted instrumentation

TABLE 2
BROADBAND COMPARISON OF BD +17°4708 FLUXES FOR STIS AND F96

Filter	F_{STIS}/F_{F96}
SDSS *u*	0.988
SDSS *g*	1.010
SDSS *r*	1.001
SDSS *i*	0.990
SDSS *z*	0.974

that plague the ground-based results. The absolute calibration of the STIS spectrophotometry is defined by the three pure-hydrogen WDs G191-B2B, GD 153, and GD 71, where NLTE model atmosphere computations establish the shapes of their flux distributions. The absolute flux levels are set by their V magnitudes relative to Vega, which has the Megessier (1995) normalization of 3.46×10^{-9} ergs cm^{-2} s^{-1} Å^{-1} instead of the H85 value of 3.44×10^{-9} at 5556 Å. The average sensitivity for STIS from the WD calibration is used to convert the observed count rates for BD +17°4708 to absolute fluxes, which can be compared with the fluxes from F96 by means of synthetic photometry.

The five SDSS filters provide examples of broad bands that cover the F96 wavelength range; Table 2 lists the ratio of the STIS to the F96 fluxes as averaged over the bandpasses via synthetic photometry calculations. The SDSS filter throughput curves[2] include the atmospheric extinction for 1.3 air masses. In order to compute the integral over the SDSS *z* filter, which has transmission beyond the STIS cutoff at 10200 Å, the last four Fukugita flux points beyond 10200 Å are concatenated with the STIS spectral energy distribution. In summary, the broadband synthetic photometry from the STIS and F96 energy distributions agrees within the quoted 0.03 mag uncertainty of F96. To the extent that the SDSS calibration depends on the flux distribution of BD +17°4708, the final column of Table 2 contains our suggested revisions to the SDSS zero-point definitions of absolute flux. Figure 2 illustrates the two sets of absolute flux distributions in the regions of peak throughput for the five SDSS filters. The differences in the flux distributions reach a maximum of 3% at 4600 Å.

Our composite standard-star spectrum extends from 0.168 to 1.200 μm and can be obtained from the CALSPEC Web site[3] along with the remainder of the *HST* standard-star library (BG04; Bohlin et al. 2001). The binary FITS table named bd17d4708_stis_001.fits has 2840 wavelength points and seven columns. An ASCII version of the flux distribution in presented in Table 3, along with the corresponding ASCII flux distribution for Vega from BG04 in Table 4. Tables 3 and 4 contain the wavelength in angstroms and the flux in ergs cm^{-2} s^{-1} Å^{-1} in the first two columns, while columns (3)–(4) are the Poisson and systematic uncertainty estimates in flux units, respectively. The last column is the FWHM of the resolution of the spectrophotometry in angstroms.

3. ACS PHOTOMETRY

The essence of an *HST* absolute flux calibration is the ratio of the count-rate response for a secondary standard to the count rate for a primary standard star with a known flux distribution. The linear CCD detector used for three STIS low-dispersion modes provides this essential ratio as a continuous function of wavelength, while ACS filter photometry independently measures this ratio in discrete bandpasses for each filter. The High Resolution Channel (HRC) and Wide Field Channel (WFC) in the ACS instrument package provide photometric images for the primary SDSS standard BD +17°4708 and for the three WD standards GD 71, GD 153, and G191-B2B. Ratios of the total stellar count rates for BD +17°4708 versus each of the three WD standards observed with the HRC and WFC provide two independent sets of confirmations of the corresponding ratios of the STIS fluxes for BD +17°4708 versus the three primary flux standards. The STIS ratios are from synthetic photometry using the total system efficiency for each ACS filter from De Marchi et al. (2004). The prescription from De Marchi et al. for bright-object photometry is also adopted, namely, 1″ aperture radius and background annuli of 5.″5–6.″5 and 6″–8″ for the HRC and WFC, respectively. Table 5 summarizes the relevant ACS observations. The observation times for BD +17°4708 in column (2) are the same for all the observations listed in column (3) except for F850LP with the HRC, where two observations of 1.8 s and four observations of 4 s are indicated. Each observation is split into two separate exposures of half the time listed in order to reject the bright pixels caused by cosmic rays.

3.1. *Details of ACS Data Reduction*

A few of the archival observations from proposals 9568 and 9661 required reprocessing with the CALACS IRAF routine because the pairs of cosmic-ray (CR-reject) images are not associated. The analysis of the final drizzled (_drz) pipeline products is complicated by difficulties in discriminating problematic data. For example, a few observations saturate the 16 bit analog-to-digital converter and must be rejected, while hot pixels are rejected in the _drz files but are generally not a real problem in the short exposures of bright standard stars. The cosmic-ray–rejected (_crj) pipeline files from the penultimate pipeline-processing step provide the same stellar photometry as the _drz files, if the pixel-area maps (PAMs) are applied. The agreement of the _crj and _drz photometry is confirmed, except for one small bug in PyDrizzle that has been fixed as of version 4.7.2. The _crj photometry corrected by the PAMs is used for the final stellar count rate values.

The CR-reject algorithm works properly only if the image pairs are aligned to a tolerance of ~0.3 pixels and have a constant point-spread function (PSF). One case (J8V601090) of HRC observations of GD 71 with F502N is split across an orbit boundary, and the PSF changed enough over the 50 minute time gap to cause multiple rejections near the core and in the first Airy ring of the PSF. The loss in total signal is about 4%. The average count rate from the separate _flt pipeline files is used for this case. Another case in which the _crj files can have erroneously low count rates is for observations where the CCD full well is filled and the excess charge bleeds along the columns. Even at the shortest available exposure time of 0.5 s, the bright star BD +17°4708 saturates WFC images and bleeds into a few pixels along a few columns, but Gilliland (2004) demonstrated linearity to better than 0.1% for such overflows of the full-well depth. However, the _flt files must be used for the photometry, because of spurious CR-rejection of pixels in the regions of the columns where the bleeding of excess charge ends.

Checking of the integral over the filter bandpass is simple for the narrowest passbands, because the stellar flux is constant over the bandpass. For example, the ratio of the count rates in F660N for BD +17°4708 to GD 71 is determined to better than

[2] From http://www.sdss.org/DR2/instruments/imager/index.html#filters.
[3] At http://www.stsci.edu/hst/observatory/cdbs/calspec.html.

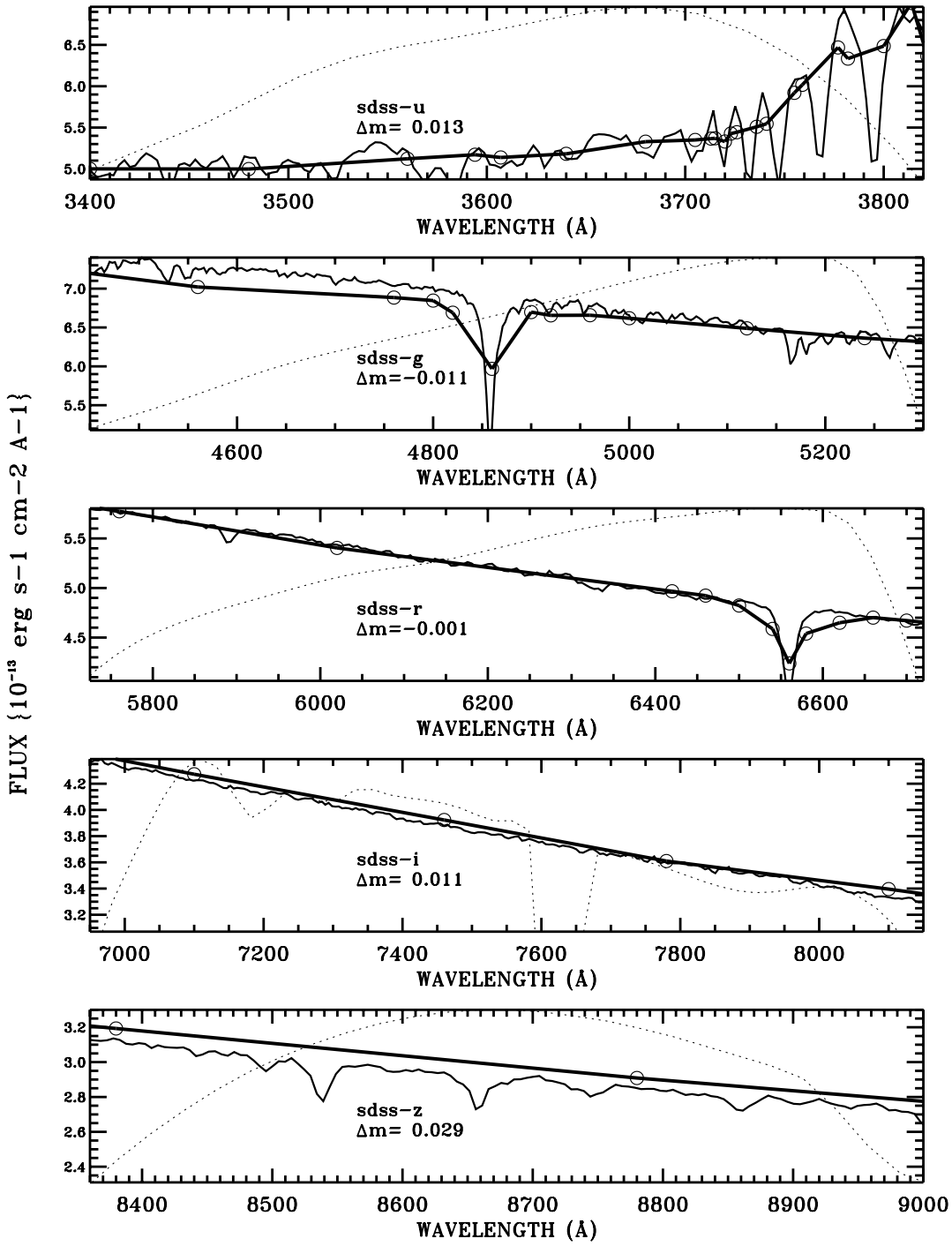

FIG. 2.—Spectral energy distribution of BD +17°4708 from STIS (*light jagged lines*) compared with Fukugita et al. (1996; *circles and heavy lines*) in the regions of peak transmission for the five SDSS filters. The light dotted lines are the transmissions of the SDSS filter curves as corrected for atmospheric extinction and normalized to the maximum value of the *y*-axes. The Δm values are from the ratios over the full bandpass in Table 2 but correlate well with the illustrated differences in the flux distributions near the peak of the filter transmissions. The biggest differences are from 4500 to 5000 Å, where STIS is up to 3% higher.

1% by inspection of the respective flux distributions. However, the ratio determined by the numerical integration differed by 2.5% from the correct value. This problem was caused by a spuriously high estimate of the out-of-band transmission in the shortest-wavelength regions near 2500 Å. The same erroneously high UV transmissions are present for several other broader filters but cause errors of less than 0.5%, even for the hottest stars. All the problematic filter transmission curves are now corrected in the STScI Synphot system (Boffi & Bohlin 2004).

3.2. *Precision of ACS Photometry*

3.2.1. *Shutter Timing Errors*

With a 0.6 ms HRC shutter timing uncertainty (Gilliland & Hartig 2003), our shortest exposures of 200 ms for BD +17°4708 in F606W are photometrically uncertain by only 0.3%. The WFC on ACS has a separate and larger shutter than the HRC, with correspondingly larger timing uncertainties. While the repeatability of the WFC shutter times is usually good to 5 ms, larger errors of as much as 14 ms are occasionally

TABLE 3

ABSOLUTE FLUX DISTRIBUTION FOR BD +17°4708

Wavelength (1)	Flux (2)	Poisson (3)	Systematic (4)	FWHM (5)
1702.33.....	4.27800×10^{-15}	2.66670×10^{-15}	4.27800×10^{-17}	2.74255
1703.70.....	5.25730×10^{-15}	2.74040×10^{-15}	5.25730×10^{-17}	2.74255
1705.08.....	1.29010×10^{-14}	3.16860×10^{-15}	1.29010×10^{-16}	2.74255
1706.45.....	1.01140×10^{-15}	2.76920×10^{-15}	1.01140×10^{-17}	2.74255
1707.82.....	9.53110×10^{-15}	2.71080×10^{-15}	9.53110×10^{-17}	2.74255

NOTE.—Table 3 is presented in its entirety in the electronic edition of the Astronomical Journal. A portion is shown here for guidance regarding its form and content.

TABLE 4

ABSOLUTE FLUX DISTRIBUTION FOR VEGA FROM BG04

Wavelength (1)	Flux (2)	Poisson (3)	Systematic (4)	FWHM (5)
900.452.....	1.23811×10^{-17}	0.00000	1.23811×10^{-19}	1.80090
901.354.....	1.67560×10^{-17}	0.00000	1.67560×10^{-19}	1.80271
902.258.....	1.78002×10^{-17}	0.00000	1.78002×10^{-19}	1.80452
903.163.....	1.82354×10^{-17}	0.00000	1.82354×10^{-19}	1.80633
904.068.....	1.86546×10^{-17}	0.00000	1.86546×10^{-19}	1.80814

NOTE.—Table 4 is presented in its entirety in the electronic edition of the Astronomical Journal. A portion is shown here for guidance regarding its form and content.

TABLE 5

ACS OBSERVATIONS

Filter (1)	Exp. Time (s) (2)	BD +17°4708 (3)	GD 71 (4)	GD 153 (5)	G191-B2B (6)	Proposal IDs (7)
			HRC			
F330W.....	6	4	2	1	2	9667, 9661
F344N	40	1	2	1	1	9667
F435W.....	1.2	1	1	1	2	9661
F475W.....	0.8	6	1	1	2	9661
F502N	24	1	1	1	1	
F550M.....	2	1	1	1	1	
F555W.....	1	1	1	1	1	
F606W.....	0.4	1	1	1	2	9661
F625W.....	0.8	6	1	1	1	
F658N	14	1	1	1	1	
F660N	40	1	1	1	1	
F775W.....	1	6	1	1	2	9661
F814W.....	0.8	1	1	1	2	9661
F850LP.....	1.8(2), 4(4)	6	1	1	1	
F892N	18	1	1	0	1	
			WFC[a]			
F475W.....	2	2	2	1	1	9020
F555W.....	2	1	2	1	1	9020
F625W.....	2	2	2	1	1	9020
F775W.....	2	2	2	1	3	9020, 9568
F814W.....	2	1	2	1	1	9020
F850LP.....	4	2	2	1	1	9020

NOTE.—Comprehensive proposals are 9664 for BD +17°4708 and 10054 for the three primary standard stars. Additional proposals with useful data are listed in the last column.

[a] WFC data exist only on chip 1 for BD +17°4708.

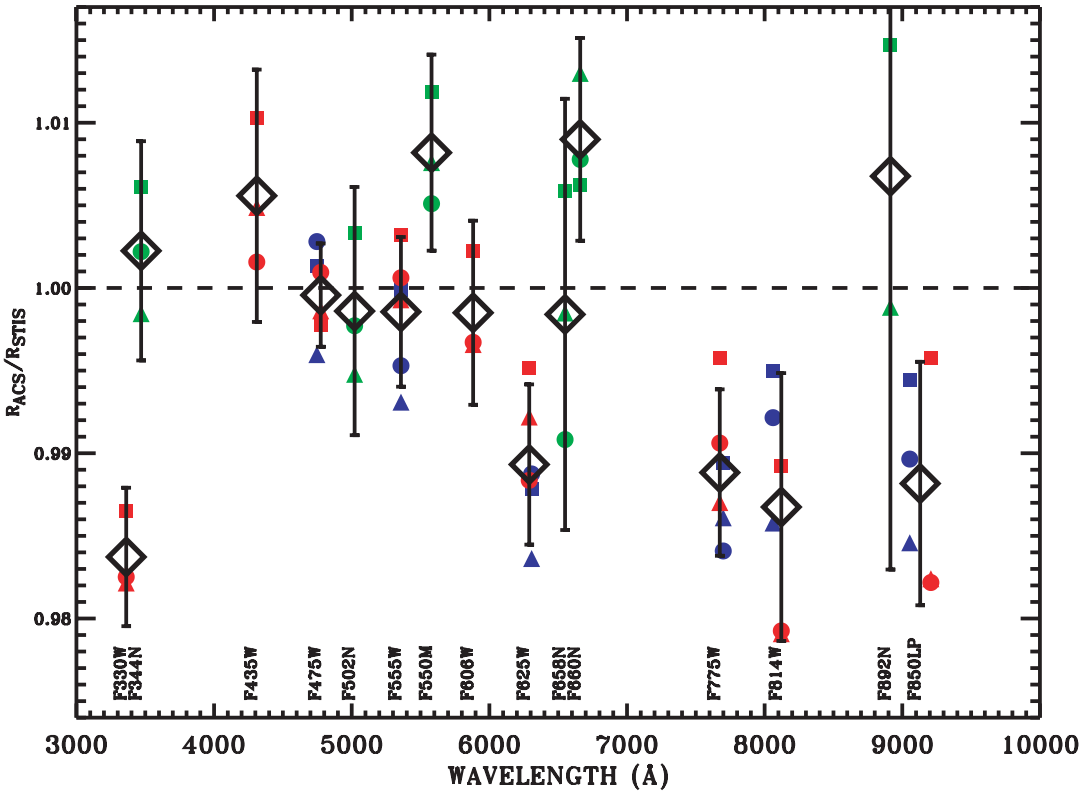

FIG. 3.—Brightness ratio of BD +17°4708 to each of the three primary WD standards for ACS, R_{ACS}, compared with the same ratio R_{STIS} derived by means of synthetic photometry from the spectral flux distributions. Blue data points are from the WFC, red are HRC broadband filters, and green are HRC narrower band filters. The ratios of BD +17°4708 to the three primary standards are shown as squares (G191-B2B), circles (GD 153), and triangles (GD 71). The large black diamonds are the averages over the three stars in both cameras for six filters and over just the three HRC data points for the other nine filters. The filter names appear near their pivot wavelengths along the bottom of the figure.

observed (Gilliland & Hartig 2003). While photometric repeatability for the WFC is generally better than 0.4% and is consistent with the typical shutter jitter of 5 ms for our exposures of 1 s and longer, a worst-case scatter of 0.92% is found among the four _flt observations of BD +17°4708 in the F625W filter. The four stellar images are all within 1″ of the same position on the detector and were all taken in a 6 minute time interval on 2002 August 4. Examination of the flat field in the region of the stellar images reveals no defects, and the four data images show no anomalies in the 1″ radius aperture. This set of four 1 s exposures must be affected by the occasional WFC shutter timing error of up to 14 ms (Gilliland & Hartig 2003). The difference between the first pair of WFC F625W exposures corresponds to a timing error of 11 ms, while the second pair differs by 16 ms.

3.2.2. *Flat-fielding Errors*

Fortunately, only the narrowband F892N filter shows any effects of interference fringes when illuminated with continuum light. Those fringes are at the 2%–3% level and could contribute to the large difference of 1.9% between the two F892N observations in Figure 3.

One measure of the quality of ACS photometry is the repeatability of identical observations. Table 5 lists five HRC filters with four to six observations of BD +17°4708 for which the repeatability is 0.63% for the 0.9 and 2 s exposure pairs (1.8 and 4 s total exposure time) with F850LP but is in the range of 0.15%–0.24% for the four shorter wavelength filters. With 1.7 million counts, Poisson statistics do not contribute substantially to the uncertainty of the 0.9 s exposures with F850LP. The larger than expected scatter for F850LP is probably caused by intermediate-scale flat-field structure that is rapidly increasing in amplitude with wavelength beyond 9100 Å (Bohlin & Hartig 2002). The position of BD +17°4708 on the HRC moved 2.″2 monotonically from (465, 480) to (526, 543), while the relative count rates showed a correlated increase of 1.8%. Because the color temperature of the star is higher than that of the tungsten lamp used to measure this intermediate-scale flat-field structure before launch, an F850LP flat field appropriate to the color of BD +17°4708 would show lower amplitude intermediate-scale structure. To minimize the effect of flat-fielding errors, only stellar images within 2″ (80 pixels) of the center of the HRC are included in Table 5.

For all the filters except F892N and F850LP, errors in photometry from flat-fielding are expected to be less than 1%. As an example of where the next-largest flat-fielding errors might arise, the F814W photometry is discussed here. To estimate the effect of positional variations on stellar photometry, the WFC F814W flat field is binned with a box size of 5×5 pixels. The WFC stellar images used in this paper are restricted to lie within 8″ (160 pixels) of a reference pixel. Typically, the stars are much closer to the reference point; for the F814W WFC, the worst deviation is for GD 153 at (3571, 1526) compared with the (3590, 1550) reference pixel. Over this small range, the binned flat field varies by less than 0.1%, so that any error due to flat-fielding should be negligible. However, for WFC the BD +17°4708 observations are centered on CCD chip 1 near a (2000, 1050) reference point, while the observations of the three WD stars are usually centered near pixel (3590, 1550) of chip 1. As an extreme upper limit to any error due to

TABLE 6
WAVELENGTH SHIFTS OF ACS FILTERS REQUIRED FOR AGREEMENT WITH STIS

Filter	F330W	F550M	F625W	F660N	F775W	F814W	F850LP
Shift (Å)	−12	+18	−24	−6.5	−44	−55	−60
Frac. of FWHM	0.020	0.033	0.017	0.16	0.029	0.022	0.049

color dependence of the flats between BD +17°4708 and the WDs, the effect of applying the F775W flat to the F814W data is computed: both flats have the same value of 0.997 at (2000, 1050), while the flat-field correction increases by 0.7% more at (3590, 1550) for F775W (1.010 vs. 1.017). Such an error of 0.7% would appear as an offset of the WFC data from the HRC for F814W in Figure 3, while the actual offset of the average of the three HRC versus the three WFC data points is consistent with this estimate. Thus, flat-fielding errors are included in the error bars on the black diamonds, as calculated from the scatter among the data points for each filter shown in Figure 3.

3.2.3. *Synoptic and CTE Errors*

Any change in sensitivity over the 1.6 yr range of the data examined here is less than a few tenths of a percent. Similar limits apply to any effect of CTE on our large 1″ aperture photometry (Riess & Mack 2004).

3.3. *Comparison of ACS Ratios with STIS*

To verify the validity of the STIS flux distribution for the *HST* secondary standard star BD +17°4708, that is, the brightness ratio with respect to the three primary pure-hydrogen WD standard stars, these ratios are also measured with ACS in several filters. To make this comparison precise, the ratio of the measured photometric count rates directly observed by ACS, $R_{\rm ACS}$, must be compared with the same ratio, $R_{\rm STIS}$, derived for the relevant ACS filters by means of synthetic photometry from the flux distributions for BD +17°4708 and for each WD. The synthetic photometric count rates are calculated according to the discussion in § 2.2 above, that is, the expected photon count rate for all four stars is computed by integrating their flux distributions in photon units over the throughput functions from De Marchi et al. (2004) for each ACS detector-filter combination. If there are no errors or unaccounted instrumental effects, then these three synthetic photometry ratios $R_{\rm STIS}$ should be equal to the corresponding measured count-rate ratios $R_{\rm ACS}$.

Figure 3 compares the observed ACS secondary (BD +17°4708) to primary (WD) brightness ratios $R_{\rm ACS}$ with the same ratio for the synthetic photometric count rates $R_{\rm STIS}$. All data points demonstrate agreement between the observed and synthetic photometric predictions to 2%, that is, $R_{\rm ACS}/R_{\rm STIS}$ is within 2% of unity. The ratios for the six available WFC broadband filters (*blue points*) fall within the scatter of the independent data from the HRC (*red points*) for the same six filters. Because the fluxes for BD +17°4708 are relative to the ensemble average over the fluxes for the three primary standards, the most relevant ratio for each filter is the average over the three stars and over the two cameras where both HRC and WFC values exist. The large black diamonds are these averages for the 15 filters, while the associated error bars are the 3 σ uncertainties in the means, where σ is defined by the scatter among the data points.

3.4. *Errors in ACS Filter Bandpasses?*

In Figure 3, there are seven filters that fall more than 3 σ from unity. One possible explanation is that the STIS flux for BD +17°4708 is in error by a smooth function that gradually drops from ∼1.005 at 4000 Å to ∼0.985 at 9500 Å. Such an error would bring all the blue WFC and most of the red HRC points into agreement. However, there are two strong arguments against this possibility. First, Figure 1 demonstrates STIS residuals of less than 0.5%. For example, around 8000 Å, where STIS rms residuals are ∼0.35%, the STIS and ACS ratios for both F775W and F814W differ by ∼1%, that is, ∼3 σ. Second, three problematic ACS filters would remain discrepant by well over 3 σ: F330W differs from the neighboring F344N by 7 σ of their combined uncertainty, and the narrower band (*green points*) F550M and F660N would increase their discrepancy to the 5–7 σ level.

Another possible explanation for the discrepant filters in Figure 3 is that the bandpasses now differ from those measured in the lab several years ago. Shifts to the blue of up to ∼100–200 Å in the long-wavelength cutoff of the SDSS *g*, *r*, and *i* interference filters are measured after installation in a vacuum dewar (S. Kent 2004, private communication). The SDSS shifts are attributed to evaporation in vacuum of water originating from ambient humidity. The ACS filters spent most of their ground-based lifetime in dry nitrogen, but some effects due to limited exposure to humidity are possible. Although the ACS shifts are also usually to the blue, the reasons for any ACS shifts must differ from the SDSS case, because the shifted ACS filters are not all blocked by interference filters on the long-wavelength edge.

With observations of only two types of flux distribution—hot blue WDs and an F star—no information is available on what filter-shape changes might have occurred. However, if the filter changes happen to be just a simple shift of the bandpass, then Table 6 illustrates the modest wavelength shifts that are required to bring the ACS ratios into agreement with the STIS ratios for the seven filters that are discrepant by more than 3 σ. The sensitivity to shifts in wavelength is caused by the difference in the slopes of the flux distributions or by the proximity to different Hα line profiles in the case of F660N. The fractional bandpass shifts ("Frac. of FWHM") are small, except for the narrow (40 Å wide) F660N. However, the −6.5 Å shift for F660N not only brings the average ACS ratio into agreement with the STIS ratio but also reverses the order of the three stars, with G191-B2B taking its usual relative position of ∼0.8% higher than the two GD stars.

4. CONCLUSIONS

To confirm the bandpass changes and distinguish between shifts of the short- or long-wavelength cutoffs of the filters, a spectrophotometric G-type standard star could be observed and analyzed in conjunction with our existing data for hot WD and F-, M-, L-, and T-type stars. If the hypothesis of filter shifts is correct, then the two sets of HRC and WFC observations have each independently confirmed the ability of STIS low-dispersion observations to establish bright secondary standards with a transfer error of less than 0.5%. The systematic trend of G191-B2B photometry (Fig. 3, *squares*) to lie above the other two stars (*circles and triangles*) suggests that the modification made by Bohlin (2000) to the Landolt *V* magnitude was ill

advised. Iteration of the STIS flux calibration is needed, which might result in a lowering of the BD +17°4708 flux level by a couple of millimagnitudes (0.2%).

J. Mack, D. Lindler, and W. Landsman provided essential assistance with the processing and reduction of the ACS observations. M. Giavalisco is principal investigator for proposal 10054, which provided the bulk of the ACS observation of the three WD standards. Primary support for this work was provided by NASA through the Space Telescope Science Institute, which is operated by the Association of Universities for Research in Astronomy, Inc., under NASA contract NAS 5-26555. Additional support came from the Department of Energy through contract C3691 from the University of California, Lawrence Berkeley National Laboratory.

REFERENCES

Boffi, F. R., & Bohlin, R. C. 2004, Revision of the Advanced Camera for Surveys Filter Throughputs (Tech. Instrum. Rep. ACS 2004-01) (Baltimore: STScI)
Bohlin, R. 1999, Changes in Sensitivity of the Low Dispersion Modes (Instrum. Sci. Rep. STIS 99-07) (Baltimore: STScI)
Bohlin, R., & Goudfrooij, P. 2003, An Algorithm for Correcting CTE Loss in Spectrophotometry of Point Sources with the STIS CCD (Instrum. Sci. Rep. STIS 2003-03R) (Baltimore: STScI)
Bohlin, R. C. 2000, AJ, 120, 437
———. 2003, in The 2002 *HST* Calibration Workshop, ed. S. Arribas, A. Koekemoer, & B. Whitmore (Baltimore: STScI), 115
Bohlin, R. C., Dickinson, M. E., & Calzetti, D. 2001, AJ, 122, 2118
Bohlin, R. C., & Gilliland, R. L. 2004, AJ, 127, 3508 (BG04)
Bohlin, R. C., & Hartig, G. 2002, HRC and WFC Flat Fields: Dispersors, Anomalies, and Photometric Stability (Instrum. Sci. Rep. ACS 2002-04) (Baltimore: STScI)
De Marchi, G., et al. 2004, Detector Quantum Efficiency and Photometric Zero Points of the ACS (Instrum. Sci. Rep. ACS 2004-08) (Baltimore: STScI)
Fukugita, M., Ichikawa, T., Gunn, J. E., Doi, M., Shimasaku, K., & Schneider, D. P. 1996, AJ, 111, 1748 (F96)
Gilliland, R. L. 2004, ACS CCD Gains, Full Well, Depths, and Linearity up to and Beyond Saturation (Instrum. Sci. Rep. ACS 2004-01) (Baltimore: STScI)
Gilliland, R. L., & Hartig, G. 2003, Stability and Accuracy of HRC and WFC Shutters (Instrum. Sci. Rep. ACS 2003-03) (Baltimore: STScI)
Hayes, D. S. 1985, in IAU Symp. 111, Calibration of Fundamental Stellar Quantities, ed. D. S. Hayes, L. E. Pasinetti, & A. G. D. Philip (Dordrecht: Reidel), 225 (H85)
Megessier, C. 1995, A&A, 296, 771
Oke, J. B., & Gunn, J. E. 1983, ApJ, 266, 713
Riess, A., & Mack, J. 2004, Time Dependence of ACS WFC CTE Corrections for Photometry and Future Predictions (Instrum. Sci. Rep. ACS 2004-06) (Baltimore: STScI)
Stys, D. J., Bohlin, R. C., & Goudfrooij, P. 2004, Time-dependent Sensitivity of the CCD and MAMA First-Order Modes (Instrum. Sci. Rep. STIS 2004-04) (Baltimore: STScI)